NeuroImage 146 (2017) 778–788

Contents lists available at ScienceDirect

NeuroImage

journal homepage: www.elsevier.com/locate/neuroimage

Decoding information about dynamically occluded objects in visual cortex

Gennady Erlikhman*, Gideon P. Caplovitz

Department of Psychology, University of Nevada, Reno, USA

ARTICLE INFO

Keywords:
Dynamic occlusion
V1
MVPA
Shape perception
Object representation

ABSTRACT

During dynamic occlusion, an object passes behind an occluding surface and then later reappears. Even when completely occluded from view, such objects are experienced as continuing to exist or persist behind the occluder even though they are no longer visible. The contents and neural basis of this persistent representation remain poorly understood. Questions remain as to whether there is information maintained about the object itself (i.e. its shape or identity) or non-object-specific information such as its position or velocity as it is tracked behind an occluder, as well as which areas of visual cortex represent such information. Recent studies have found that early visual cortex is activated by "invisible" objects during visual imagery and by unstimulated regions along the path of apparent motion, suggesting that some properties of dynamically occluded objects may also be neurally represented in early visual cortex. We applied functional magnetic resonance imaging in human subjects to examine representations within visual cortex during dynamic occlusion. For gradually occluded, but not for instantly disappearing objects, there was an increase in activity in early visual cortex (V1, V2, and V3). This activity was spatially-specific, corresponding to the occluded location in the visual field. However, the activity did not encode enough information about object identity to discriminate between different kinds of occluded objects (circles vs. stars) using MVPA. In contrast, object identity could be decoded in spatially-specific subregions of higher-order, topographically organized areas such as ventral, lateral, and temporal occipital areas (VO, LO, and TO) as well as the functionally defined LOC and hMT+. These results suggest that early visual cortex may only represent the dynamically occluded object's position or motion path, while later visual areas represent object-specific information.

1. Introduction

The motion of objects and observers through the environment often results in patterns of occlusions and disocclusions when nearer objects block those that are farther away. Sometimes, only parts of objects are occluded as when an animal is seen through foliage. Even in such extreme cases, when only a few object fragments are visible at any given time, the visual system can nevertheless accurately recover the entire shape (Palmer et al., 2006). Other times, an object may completely disappear from view before reappearing. For example, a person might walk behind a column and reemerge on the other side. Objects that are dynamically occluded in this manner are experienced as continuing to exist or persist behind the occluder even though they are no longer visible. When the object becomes visible again, the experience is of precisely that – that it is the same object that was seen a moment ago prior to its occlusion. Despite the ubiquity of dynamic occlusion in everyday perception, little is known about what it actually means for an object to persist – that is, what and how information about the object is maintained and represented while it is invisible. In this paper, we use functional magnetic resonance imaging (fMRI) to examine what information about an object is represented when it is occluded from view.

One hypothesis is that although an object's identity is maintained during occlusion, its features are not. Continuity between objects that disappear behind an occluder and those that re-emerge can be seen even when some of the object's features change. For example, a red circle that disappears behind an occluder and a green square that reappears on the other side may be perceived as the same, continuously moving object. This phenomenon has been called the "tunnel effect" (Burke, 1952; Flombaum and Scholl, 2006; Flombaum et al., 2008; Michotte et al., 1964). Object identity in the tunnel effect is more strongly determined by spatiotemporal continuity than by the surface features of the object, suggesting that object identity may not be strongly tied to its surface features (Bahrami, 2003; Feldman and Tremoulet, 2006; Flombaum and Scholl, 2006; Flombaum et al., 2008; Gao and Scholl, 2010; Howard and Holcombe, 2008; Kahneman et al., 1992; Oksama and Hyönä, 2008; Papenmeier et al., 2013; Pylyshyn, 2001, 2004; Saiki, 2003; Scholl and Pylyshyn, 1999). Likewise, during

* Corresponding author.
E-mail address: gennaer@gmail.com (G. Erlikhman).

http://dx.doi.org/10.1016/j.neuroimage.2016.09.024
Received 26 May 2016; Accepted 11 September 2016
Available online 20 September 2016
1053-8119/

multiple object tracking, observers can identify moving targets that they had been tracking amongst several distractors, but they cannot recall which target had which previously assigned name (Pylyshyn, 1989).

The tunnel effect also shares some similarity with long-range apparent motion, in which motion can be seen between two successively flashing objects that do not match in surface features (Exner, 1875; Kolers, 1964; Kolers and Pomerantz, 1971; Korte, 1915; Navon, 1976; Prazdny, 1986; Wertheimer, 1912). Early theories of long-range apparent motion suggested that a nonspecific, "blob-like" representation is formed along the path of apparent motion and that it is this simple token that is then matched across successive instances based on spatiotemporal proximity (Attneave, 1974; Ullman, 1980; Marr, 1982). Motion tokens have also been invoked to explain interactions along the apparent motion path (Yantis and Nakama, 1998) as well as the perception of apparent motion between bounded regions (Stanley and Rubin, 2003, 2005). Such abstract representations may also underlie the persistence of objects during dynamic occlusion without a specific representation of its features.

An abstract, motion-path-like representation is consistent with findings from several studies that examined the neural areas involved in the representation of completely occluded objects which found activation in higher-level visual areas like the intraparietal sulcus (IPS), MT, and LOC (Assad and Munsell, 1995; Baker et al., 2001; Hulme and Zeki, 2007; Makin et al., 2009; Olson et al., 2003; Shuwairi et al., 2007). For example, Olson et al. (2003) measured fMRI activity while subjects watched a ball pass behind an occluder. The ball either became gradually occluded or disappeared all at once when it came into contact with the occluder and then either gradually or instantly reappeared on the opposite side and continued along its motion path. Stronger activation was observed in the IPS and MT during occlusion for gradually occluded objects than for either disappearing of static objects, suggesting that object motion was represented in those areas during occlusion. Instantaneous disappearance was thought to disrupt the formation of an occluded motion signal. Hulme and Zeki (2007) conducted a similar experiment in which houses and faces were either gradually occluded by a nearer surface or instantaneously disappeared. Greater activation was found for faces in FFA and houses in the LOC during occlusion than when they instantly vanished. Because stimuli were visible prior to occlusion and vanishing, the difference in activation was attributed to the continued representation of the object or "the awareness of the object's presence" during occlusion. Neither study speaks to whether any object features beyond their category and motion path are represented.

However, several recent studies suggest that some low-level object properties may be represented during occlusion. Flombaum et al. (2008) found that an object's spatial extent was maintained during occlusion using a dot probe task during multiple object tracking. Similarity and dissimilarity between object features can also determine their degree of binding to objects, suggesting that features are actively being represented (Caplovitz et al., 2011; Hein and Moore, 2012). Feature-based grouping can also occur during multiple object tracking and is sometimes used automatically by the visual system to either facilitate or impair tracking performance (Erlikhman et al., 2013; Keane et al., 2011). Although no studies to our knowledge have examined whether low-level object features may be represented during dynamic occlusion, studies of apparent motion in which there is also an invisible object in an unstimulated region of space have repeatedly identified a role of early visual cortex in the representation of objects or their properties along the apparent motion path (Chong et al., 2015; Goebel et al., 1998; Kaneoke et al., 1997; Larsen et al., 2006; Maus et al., 2010; Muckli et al., 2005; Seghier et al., 2000; Sterzer et al., 2006; Wibral et al., 2008). Activation of early visual cortex has likewise been observed for objects that are not physically present during visual imagery (Albers et al., 2013; Klein et al., 2000; Slotnick et al., 2005). Dynamically occluded objects may therefore be represented with high fidelity throughout the visual representational hierarchy, including in early visual areas.

Studies examining dynamic occlusion either did not look at early cortical areas or compared activity to an unoccluded condition and unsurprisingly found greater activation to unoccluded objects in early visual areas than to occluded ones (Shuwairi et al., 2007). Furthermore, even in higher-level visual areas that are activated during dynamic occlusion, the nature of the representation is unknown: whether activity in those areas reflects merely the awareness that something is occluded, or its category, or information about the object's motion path (including its position and velocity), or more specific shape or form information.

In order to examine the cortical signatures of dynamically occluded objects, we presented subjects with different objects (circles and stars) that moved through and were occluded in distinct quadrants of the visual field. This design allowed us to isolate functional MRI activity corresponding to regions where the object was visible and moving and those where the object was occluded and completely invisible. Similar to Olson et al. (2003), objects either instantly disappeared upon reaching the occlusion quadrant or became gradually occluded (i.e., passed behind the occluder). We hypothesized that if there is activity in early visual areas (V1-V3) during dynamic occlusion, and if that activity includes a representation of the object's features, then object identity should be decodable in those areas. Otherwise, if the representations are less precise and more "blob-like", there may be activity in early cortical areas that corresponds to the object's motion or presence, but the corresponding pattern of activity would not contain the form information necessary for distinguishing between different kinds of objects. However, there may be object identity preserved in higher visual areas such as LOC (Hulme and Zeki, 2007). As a preview of the results, activation corresponding to dynamic occlusion was found in early visual cortex (V1-V3), for gradually occluded, but not for instantly disappearing objects. However, using several measures, object identity could only be decoded in later visual areas and not in early ones. We interpret the activity in early visual areas during dynamic occlusion as indicative of information representing object position, its motion path, or the path of attention. In contrast, the role of higher visual areas is to maintain a representation of the object's identity including some form information. We speculate that the precise spatiotemporal information represented in early visual cortex allows higher-level object specific information to be rapidly updated once the object re-emerges from occlusion without necessitating a *de novo* object representation. This may account for why spatiotemporal continuity can be perceived between objects that change features while occluded as in long-range apparent motion.

2. Materials and methods

2.1. Participants

Ten observers (two female, eight male; 28-45 years of age) participated in the experiment. All observers were right-handed, reported normal or corrected-to-normal vision, and reported no history of neurological disorders. Observers provided written consent. Observers participated in four scanning sessions: one for a high-resolution anatomical image, one for retinotopic mapping, and two for the two experimental conditions, disappearance and occlusion (see below). Some data were collected from an additional four observers, but were not included either due to attrition (not finishing all of the scanning sessions) or due to data collection errors during scanning. Participants were compensated $50 per hour for their participation.

2.2. The main experiments

We first present the general logic and motivation of the experiment and analyses and then present the experimental details.

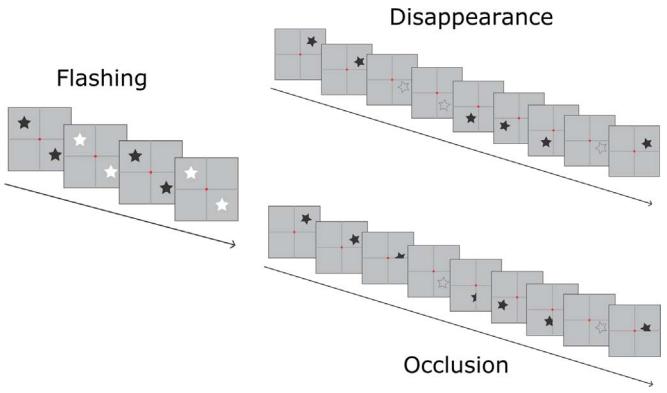

Fig. 1. Sequence of frames depicting what participants saw in the experiment. Shapes were either stars or circles. The dark gray lines dividing the display into quadrants are for illustrative purposes only, and were not visible during the experiments. On the left, the flashing localizer – shapes alternated between white and black in the upper-left and lower-right quadrants. On the right, the two motion conditions. Objects travelled along a circular path from the upper-right to the lower-left quadrant and back several times. In the disappearance condition, when the object reached the lower-right quadrant, it instantly disappeared, indicated by the outline shape in the figure. In the occlusion condition, the shape became gradually occluded as it entered the lower-right quadrant and was gradually revealed as it exited that quadrant. We refer to the lower-right quadrant as the dynamic occlusion or occluded quadrant and the upper-left quadrant as the unstimulated control quadrant.

Dynamic occlusion was created by having an object – a circle or a star – travel from the upper-right to the lower-left quadrant of a display, disappearing or becoming occluded in the lower-right quadrant (motion condition). The resulting percept was of continuous motion through the lower-right quadrant even though the object was not visible anywhere in that area. Large objects were used instead of Gabor patches or line segments because we wanted to minimize any cortical activation that may have arisen due to lateral horizontal connections in early visual cortex (Seriès et al., 2003; for review see Fregnac et al. (2009)). Division of the display area into quadrants allowed us to selectively examine activity in retinotopic cortical areas that corresponded to regions of the display through which the object was moving and visible (upper-right and lower-left), areas that corresponded to the non-stimulated, occlusion quadrant that contained the occluded object (lower-right), and a non-stimulated control quadrant (upper-left) through which the object never moved (see Fig. 1).

We first examined whether there was any activation in early visual areas during dynamic occlusion (see Univariate Analysis below). In order to address the more difficult question of representation, an object localizer (flashing condition) was used to select voxels along the motion path in the occlusion quadrant and in the unstimulated control quadrant that were activated by stationary circles and stars that were flashed in those quadrants in a separate block. Multi-voxel pattern analysis (MVPA) was then used to attempt to decode object identity from patterns of activation during dynamic occlusion (i.e., cross-classification with the motion condition). A classifier was trained on patterns of activity created by the flashing, static objects and was used to decode object identity during occlusion. Static instead of moving objects were used to create the localizer so that the selected voxels would correspond exclusively to contour, position, and shape information, and not the object's motion. Because the classifier was trained on this activity, discrimination between circles and squares moving through the quadrant could not be attributed to differences in their motion paths or other aspects of their motion.

2.2.1. Stimuli and experimental design

The display consisted of a gray background divided into four, unmarked quadrants. There were two stimulus presentation conditions – moving and flashing – that occurred in different quadrants. Two shapes were used: a circle and star. The circle had a diameter of 4.34° of visual angle and the star had a maximum width and height of 6.46°. The surface area of the circle was matched to that of the star. In the motion condition, a black object appeared in the upper-right quadrant and moved clockwise along a circular path about the center of the screen at a rate of 90°/s until it reached the horizontal meridian separating the upper-right and lower-right quadrants. In the disappearance condition, the object disappeared instantaneously upon reaching the meridian, and then reappeared at the vertical meridian between the lower-right and lower-left quadrants after a delay of 200 ms and continued along its clockwise path. Once the object reached the horizontal meridian separating the lower-left and upper-left quadrants, the object reversed direction, and retraced its path, disappearing in the lower-right quadrant and reappearing in the upper-right. As a result, the object was visible only in the upper-right and lower-left ("motion") quadrants and was never visible in lower-right ("occlusion") or the upper-left ("control") quadrants. This movement was repeated continuously for the duration of the entire block. Over the course of a single block, objects passed through the occlusion quadrant eight times.

In the occlusion condition, the display was exactly the same except that instead of disappearing, the object continued to move into the lower-right quadrant, becoming gradually occluded. There were no features to indicate the presence of the occluding surface. However, objects passed through the occlusion quadrant several times during the course of a single block and that quadrant was always the occluded one. In the flashing condition, two objects were presented, one each in the center of the upper-left and lower-right quadrants. The object alternated between black and white at a rate of 10 Hz. A stimulus block contained either the star or the circle in both quadrants. The disappearance, occlusion, and flashing condition are depicted in Fig. 1 and can be seen in Movie 1.

Supplementary material related to this article can be found online at http://dx.doi.org/10.1016/j.neuroimage.2016.09.024.

A run consisted of interleaved stimulus (16 s) and blank blocks (12 s). All four types of stimulus blocks – two shape conditions (circle and star) and two presentation conditions (flashing and motion) – appeared twice per run. A balanced Latin square design was used to determine stimulus block order across eight total runs per experiment. Blank blocks were included at the start and end of each run and between each stimulus block so that each stimulus block was preceded and followed by a blank block. During a blank block, only the fixation point was shown on a gray background. In total, a run consisted of nine blank blocks and eight stimulus blocks. Disappearance and occlusion conditions were run in separate scanning sessions.

During each run, subjects performed a change-detection fixation task to ensure that they maintained focus during the experiment. On each frame, there was a 5% chance that a fixation dot changed color from red to green for 300 ms. Subjects had 500 ms to press a button on a button box to indicate that they detected the color change. There was an enforced minimum delay of 5 s between each color change. Color changes occurred during both stimulus and blank blocks. At the end of each run, subjects were shown their average task performance for that run.

2.3. MRI apparatus and scanning procedures

Retinotopic data were acquired at the University of California, Davis Imaging Research Center on a 3T Skyra MRI System (Siemens Healthcare, Erlangen, Germany) using a 64 channel phased-array head coil. Functional images were obtained using T2* fast field echo, echo planar functional images (EPIs) sensitive to BOLD contrast (TR=2.5 s, TE=25 ms, 32 axial slices, 3.0 mm^2, matrix size=80×80, 3 mm thickness, interleaved slice acquisition, 0.5 mm gap, FOV=240×240, flip angle=71°). High-resolution structural scans were collected to support reconstruction of the cortical hemisphere surfaces using FreeSurfer from T1 (MPRAGE, TR=2230 ms, TE=4.02 ms, FA=7°, 640×640

matrix, res=0.375×0.375×0.8 mm) and T2 (TR=3 s, TE=304 ms, FA=7°, 640×640 matrix, res=0.375×0.375×0.8 mm) images.

Experiment data were acquired at the Neuroimaging Facility of Renown Health Hospital in Reno, NV on a 3T Philips Ingenia scanner (software version 4.1.1) using a 32-channel digital SENSE head coil (Philips Medical Systems, Best, Netherlands). Functional images were obtained using T2* fast field echo, echo planar functional images (EPIs) sensitive to BOLD contrast (TR=2 s, TE=25 ms, 32 axial slices, 3.0 mm^2, matrix size=80×80, 3 mm thickness, interleaved slice acquisition, 0.5 mm gap, FOV=240×240, FA=71°).

For both retinotopy and experimental data collection, the stimulus computer was a 2.53 GHz MacBook Pro with an NVIDIA GeForce 330 M graphics processor (512MB of DDR3 VRAM). Stimuli were generated and presented using the Psychophysics Toolbox (Brainard, 1997; Pelli, 1997) for MATLAB (Mathworks Inc., Natick, MA). Retinotopic stimuli were presented on a 24 in. Cambridge Research System (Kent, UK) LCD BOLDscreen display (60 Hz refresh rate) outside of the scanner bore and viewed with a tangent mirror attached to the head coil, which permitted a maximum of visual area of 19.3°×12.1°. Experiment stimuli were presented using a 32 in. SensaVue (85 Hz refresh rate) visual display system (Invivo, Inc., Gainesville, FL) outside of the scanner bore and viewed with a tangent mirror attached to the head coil, which permitted a maximum of visual area of 31.5°×18.9° In all experiments, stimulus presentation was time locked to functional MRI (fMRI) acquisition via a trigger from the scanner at the start of image acquisition.

2.4. Data preprocessing

Functional fMRI data were analyzed using AFNI (http://afni.nimh.nih.gov/afni/; Cox, 1996), SUMA (http://afni.nimh.nih.gov/afni/suma, Saad et al., 2004), FreeSurfer (http://surfer.nmr.mgh.harvard.edu; Dale et al., 1999; Fischl et al., 1999), MATLAB, and SPSS Statistics 22 (IBM, Armonk, NY). Functional scans were slice-time corrected to the first slice of every volume and motion corrected within and between runs. The anatomical volume used for surface reconstruction was aligned with the motion-corrected functional volumes and the resulting transformation matrix was used to provide alignment of surface-based topographic ROIs with the experiment datasets.

2.5. Retinotopic mapping

The retinotopy methods were the same as those used in Erlikhman et al. (In Press). We reprint them here verbatim.

A color and luminance varying flickering checkerboard stimulus was used to perform standard retinotopic mapping (Swisher et al., 2007; Arcaro et al., 2009; Killebrew et al., 2015). Participants performed 8 runs of polar angle mapping and 2 runs of eccentricity mapping. For both polar angle and eccentricity mapping, participants were instructed to maintain fixation on a central spot while covertly attending to a rotating wedge (45° width, 0.5°–13.5° or 8°–13.5° eccentricity, 40 s cycle, alternating clockwise and counterclockwise

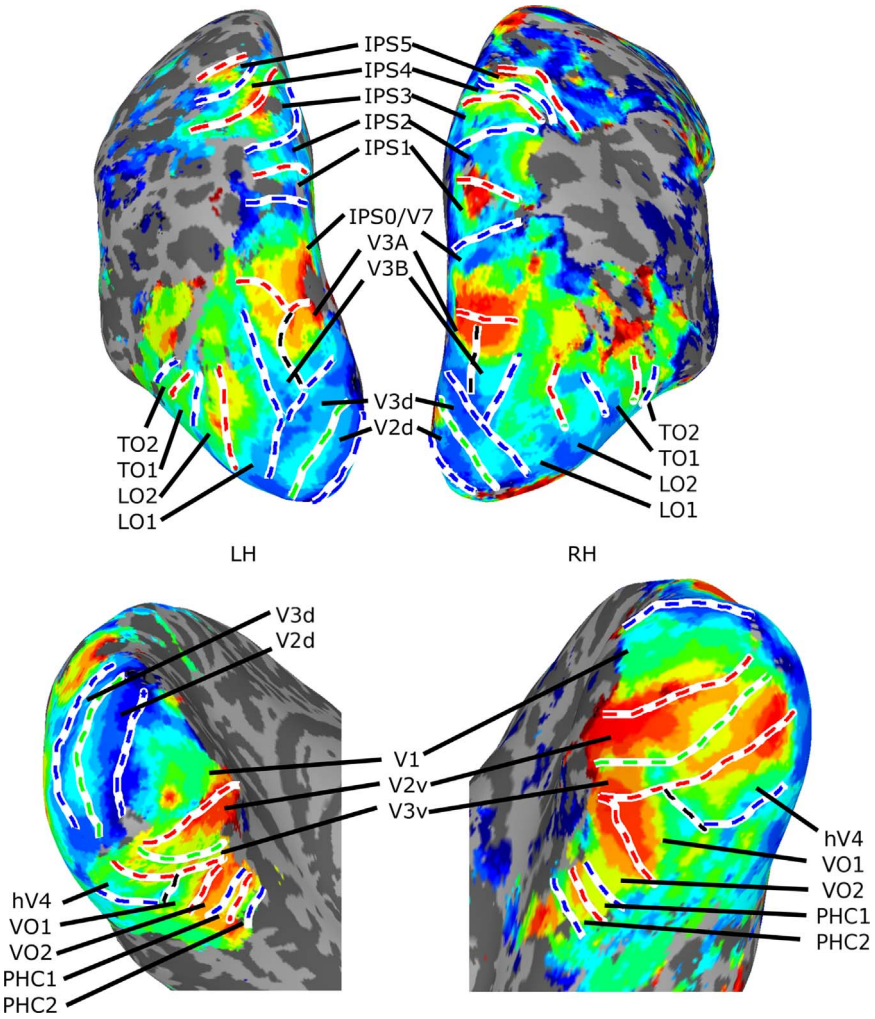

Fig. 2. Regions of interest (ROIs) for both hemispheres for a sample subject. Figure from Erlikhman et al., (2016). The neural representation of objects formed through the spatiotemporal integration of visual transients. *NeuroImage*.

rotation across runs) or expanding/contracting ring (1.7° width, traversing 0°–13.5° eccentricity, 40 s cycle plus 10 s blank between cycles, alternating expanding and contracting direction across runs) stimulus and to report via a button press the onset of a uniform gray patch in the stimulus that served as that target. Targets appeared, on average, every 4.5 s.

Polar angle and eccentricity representations were extracted from separate runs using standard phase encoding techniques (Bandettini et al., 1993; Sereno et al., 1995; Engel et al., 1997). For each participant, we defined a series of topographic ROIs on each cortical hemisphere surface using AFNI/SUMA. Borders between adjacent topographic areas of the intraparietal sulcus were defined by reversals in polar angle representations at the vertical or horizontal meridians as described in Wang et al. (2015) using standard definitions (Sereno et al. 1995; DeYoe et al., 1996; Engel et al., 1997; Press et al., 2001; Wade et al., 2002; Brewer et al., 2005; Larsson and Heeger, 2006; Kastner et al., 2007; Konen and Kastner, 2008; Amano et al., 2009; Arcaro et al., 2009; for review, see Silver and Kastner (2009), Wandell and Winawer, 2011). In total, we defined 23 topographic regions: ventral and dorsal V1-V3, hV4, VO1-2, PHC1-2, V3A, V3B, LO1-2, TO1-2, and IPS0-5.

2.6. Functional ROIs

In addition to the topographic regions, four functional ROIs were defined: fusiform face area (FFA), parahippocampal place area (PPA), lateral occipital complex (LOC), and human analog of the medial temporal region (hMT+). A standard object category localizer was used to define FFA, PPA, and LOC (Malach et al., 1995; Grill-Spector et al., 1998). Subjects were shown grayscale pictures of objects from four categories (faces, houses, generic objects, and scrambled generic objects) in 15 s blocks containing 20 stimuli each (350 ms duration, 400 ms inter-stimulus interval). Each category contained 40 unique images from which the images used in each block were selected. In a session, there were 4 runs with 3 blocks of each stimulus category per run. The stimuli subtended approximately 12° vertically and horizontally. While maintaining central fixation, subjects performed a one-back, responding when a stimulus was repeated twice in a row. The FFA was defined as the region that showed greater activation ($p < 0.01$) to faces than any of the other categories (Kanwisher et al., 1997; Haxby et al., 1999), the PPA as the region that showed greater activation to houses rather than faces within the collateral sulcus (Epstein et al., 1999), and the LOC as the region that showed greater activation to intact compared to scrambled objects.

A standard motion localizer was used to define hMT+. Subjects were shown either static or moving, limited-lifetime white dots with a diameter of 0.15° on a black background. The dots were drawn within an area 15° centered on the middle of the screen. When moving, dots moved either outward or inward at a rate of 8°/s. There were 1000 dots in total. When a dot left the drawing area, it was recreated in a new, random position somewhere within the allowed area. Subjects fixated on a central, static white dot and performed a color change detection task. The fixation dot dimmed from white to red for 90 ms once every 2–5 s and subjects had to press a key whenever they noticed the change. hMT+ was defined as the region that showed greater activation to moving as compared to static displays. Functional localizers were not available for one subject and this subject was excluded from these analyses. The ROIs are shown for one representative subject in Fig. 2.

2.7. General linear model, selection of voxels, and definition of regions of interest

For each voxel, functional images were normalized to percent signal change by dividing the voxel-wise time series by its mean intensity in each run. The response during each of the four conditions (circles flashing, circles moving, stars flashing, stars moving) was quantified in the framework of the general linear model (Friston et al., 1995). Square-wave regressors for each of the four unique conditions were generated and convolved with a model hemodynamic response function (BLOCK model in AFNI's 3dDeconvolve function) accounting for the shape and temporal delay of the hemodynamic response. Nuisance regressors were included to account for variance due to baseline drifts across runs, linear and quadratic drifts within each run, and the six-parameter rigid-body head motion estimates. The resultant beta weights derived for each of the conditions of interest represent the observed percent signal change in response to the corresponding stimulus. For the subsequent multivariate pattern analyses, the general linear model was applied separately for each run. In order to localize voxels of interest in the un-stimulated quadrants of the motion conditions, a single general linear model using the combined data of all eight runs was applied.

By taking advantage of the small receptive fields and topographically segregated quadrant representations of V1, V2 and V3, we were able to define our primary voxels of interest as those in the left hemisphere V1d, V2d and V3d corresponding to occlusion quadrant and those in the right hemisphere V1v, V2v and V3v corresponding to the control quadrant for which the flashing stimuli (both stars and circles combined) elicited positive beta weights at a *t*-statistic threshold of 1.96. These localizers were created separately for each of the two experimental sessions (disappearance or gradual occlusion).

Additional voxels of interest were defined in higher-order topographically organized areas hV4, VO1-2, PHC1-2, LO1-2, TO1-2, V3A, V3B, IPS0-5 and in the functionally-defined areas FFA, PPA, LOC, and hMT+. The voxels selected were those in the left hemisphere (right hemifield) for which the flashing stimuli (both stars and circles combined) elicited a greater activation than the motion stimuli.

3. Data analysis

3.1. Univariate timecourse analyses during dynamic occlusion

A separate general linear model was applied using the combined data of all eight runs in which the finite impulse response was derived for each condition starting from 4 s prior to and extending 28 s following the start of each block (TENT model in AFNI's 3dDeconvolve function). For each voxel, an activity timecourse was derived for all four conditions (flashing and moving stars and circles). The timecourses for each voxel within a given region of interest were then averaged together. This resulted in a single waveform for each condition and ROI. The voxels selected were those that exceeded a threshold level of activation in the flashing condition (see above). For example, within the left hemisphere V1d, the timecourses for each voxel localized in the flashing conditions were averaged together to create a single waveform for the dynamic occlusion conditions. Timecourses were also derived from voxels in the right hemisphere V1v corresponding to the control quadrant. Thus for each topographically or functionally defined ROI there were matched timecourse waveforms corresponding to the quadrant in which the object was dynamically occluded and the control quadrant which never contained a moving or occluded object. A difference wave was then computed between these two timecourses: the waveforms for the motion conditions in the control regions of unstimulated space (i.e. right hemisphere V1v) were subtracted from the waveforms for the motion conditions corresponding to the dynamically occluded quadrant (i.e. left hemisphere V1d). The resulting waveform is the difference in activation between two *unstimulated* quadrants.

3.2. Multivariate pattern analysis

The univariate analysis described above was designed to detect whether there was greater activity during dynamic occlusion compared to control regions of unstimulated space. In order to examine the

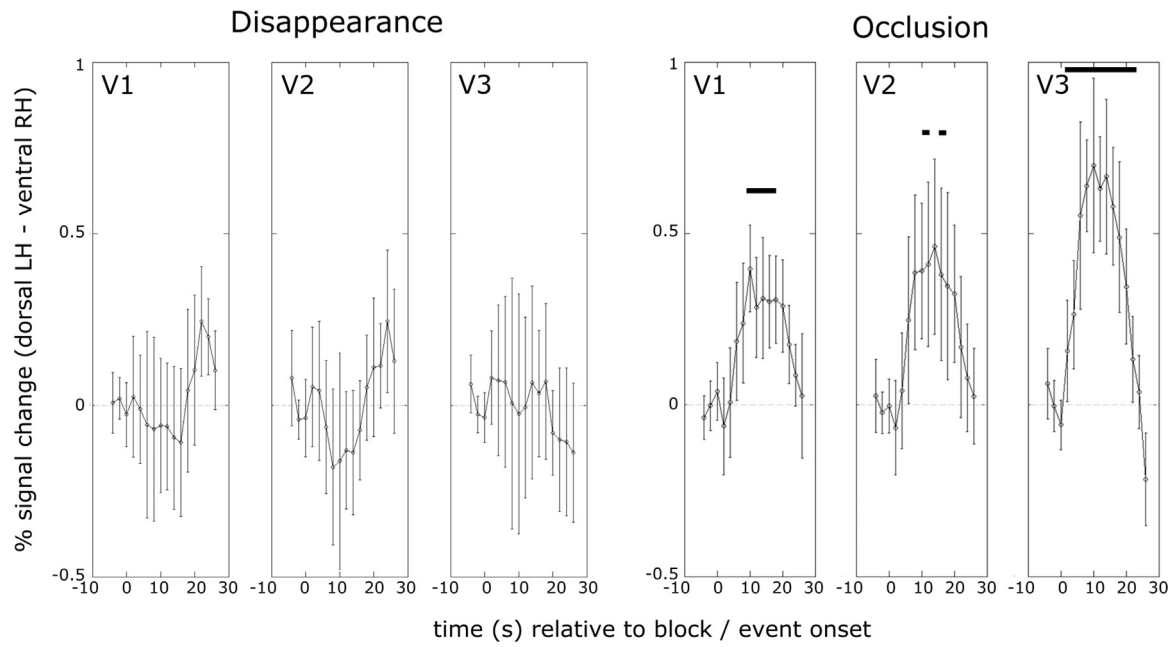

Fig. 3. Group-average difference in activation between voxels corresponding to the quadrant containing the apparent motion path (lower-right – dorsal, left hemisphere) and the quadrant in which there was no motion (upper-left – ventral, right hemisphere) for disappearing (left) and occluded (right) objects (averaged across circles and stars). Voxels were selected topographically (V1, V2, and V3) and using the flashing localizer, so that the difference reflects activity during motion in voxels that were active during flashing. Error bars are 95% confidence intervals. The horizontal black bars indicate time points which were significantly different from 0 (one-tailed, signed rank test, corrected for multiple-comparisons).

nature of what information may be represented during dynamic occlusion, we performed a series of multivariate pattern analyses using the run-wise beta weights for each condition. Three linear SVM classifiers (Cortes and Vapnik, 1995) were used to discriminate the circle and star objects during flashing and motion conditions within each ROI. The first classifier was trained and tested on flashing objects using leave-one-out cross-validation. The classifier was trained on seven of the eight runs and tested on the remaining run. This was repeated for each run and the final classifier performance was the average across all cross-validation folds. This classifier was used to establish whether there was sufficient shape information in V1-V3 to perform subsequent classifications of occluded objects. The remaining two classifiers were also trained on patterns of activation during flashing, but were tested on the patterns of activation during motion in the occlusion quadrant for both disappearing and occluded objects. This cross-classification was necessary to isolate the representation of form or identity information during occlusion and to distinguish it from motion signals that could have discriminated between the two objects. No cross-validation was performed for these classifiers because the training and testing datasets were non-overlapping.

A bootstrap permutation test was performed to evaluate statistical significance independently for each ROI for all classifiers. For each subject, a dataset-wide (Etzel and Braver, 2013; Etzel, 2015) permutation was applied 10,000 times by randomizing the data labels within each run, keeping the same number of circle and star labels per run as in the original dataset. These scores were then averaged across subjects, yielding 10,000 group-average scores based on permuted data. The observed average accuracy on the original dataset was then ranked relative to this distribution of permuted scores in order to compute a p value, p_{perm}.

In addition to the SVM analysis, we also performed a correlation-based multivariate pattern analysis. If any shape information was maintained during dynamic occlusion when no object was physically present, that pattern of activity ought to have a greater correlation with the same object when it was visible in the same part of the display (i.e. during the flashing condition) as opposed to the other object. For example, the pattern of activity in the voxels that were selective for a flashing star would be more similar to the activation when a star was moving behind an occluder in that same quadrant than when a circle was moving through the same area (even though both displays were identical in the sense that nothing was presented in that quadrant). We refer to this measure of shape information as Δr (see Peelen et al. (2009)):

$$\Delta r_{star} = corr\,(star_{move}, star_{flash}) - corr\,(star_{move}, circle_{flash})$$
$$\Delta r_{circle} = corr\,(circle_{move}, circle_{flash}) - corr\,(circle_{move}, star_{flash})$$

In the dynamic occlusion quadrant, if shape information was preserved, we expected the measure to be positive (i.e., greater correlation during motion and flashing for the same shape than between shapes). If no information was preserved, the measure would be zero. The measure was computed separately for the two objects. Unlike the MVPA analysis which used the flashing information for training and the motion information for testing, the correlation analysis combines both sets of data for its measure and may therefore be more sensitive to shape information.

For all analyses, multiple comparison testing was documented by computing the false discovery rate (FDR) separately for each analysis using Storey's procedure (Storey 2002; Storey and Tibshirani, 2003). A default value of λ=0.5 was used to estimate π_0 (Krzywinski and Altman, 2014). Whenever π_0 was 0 (e.g. because all tests were significant), a more conservative setting of π_0=1 was used, which corresponds to the original Benjamini-Hochberg procedure (Benjamini and Hochberg, 1995; Benjamini and Yekutieli, 2001).

4. Results

4.1. Behavioral results

All subjects were able to detect the fixation point change with a high degree of accuracy across all experimental runs in both experiments. The range of accuracies was 93.54–100% (mean: 98.65%) for disappearing and 95.98–100% (mean: 99.24%) for occluded objects. There were no significant differences in task performance across the four stimulus types and blank intervals for either disappearing ($F_{4,32}$=0.853, $p > 0.50$, η^2_p=0.096) or occluded ($F_{2.16,19.45}$=1.21, $p > 0.32$, η^2_p=0.119, Greenhouse-Geisser corrected) objects, suggesting

that subjects maintained fixation and paid close attention to events at the central fixation point throughout the experiment.

4.2. Timecourse analyses

Fig. 3 shows the difference in activation between the critical quadrants of interest: the lower-right, dynamic occlusion quadrant and the upper-left, control quadrant, which corresponded to left dorsal and right ventral V1-V3 respectively. For disappearing stimuli, there was no difference in activity during the motion conditions. However, for gradually occluded objects, in all three early visual ROIs, there was greater activation during motion in the dynamic occlusion quadrant than in the control quadrant.

To verify that the activation observed during dynamic occlusion was due to the passing of an object behind an occluder, two control analyses were performed and are described in greater detail in the Supplementary Materials. First, response to flashing objects was compared between ROIs that corresponded to the two quadrants in which objects flashed (lower-right, dynamic occlusion and upper-left, control quadrant). This control analysis tested whether the observed effects in the occluded quadrant were due to an asymmetry in responsiveness in ventral and dorsal ROIs. There were no differences in activation in any of the three ROIs between the dynamic occlusion and control quadrants (Fig. S1) when the objects were flashing in those quadrants. For the second control, the analysis was repeated in restricted, manually defined ROIs that covered only the central regions of V1-V3 excluding any voxels located near the horizontal meridian (Fig. S2). When objects gradually disappeared behind the occluder, portions of the objects were visible for longer near the boundary of the occluded quadrant than when objects instantly disappeared when they reached the boundary. Furthermore, as the objects became occluded, they could have been perceptually completed behind the occluder, stimulating voxels within the dynamic occlusion quadrant (Ban et al., 2013; Halko et al., 2008; Shipley and Kellman, 2003; Singh and Fulvio, 2007). It was therefore important to exclude any voxels in that quadrant that may have been activated when the object was still visible. A qualitatively similar pattern of results for the occlusion condition was found when looking only at voxels in the center of each ROI, which were less likely to be activated by the presence of an object near the meridian separating the upper and lower visual fields (Fig. S3).

In summary, we found activation in early visual cortex corresponding to a dynamically occluded object similar to what has recently been found with apparent motion (Chong et al., 2015; Larsen et al., 2006; Muckli et al., 2005; Sterzer et al., 2006). However, when the object instantly disappeared instead of becoming gradually occluded, there was no evidence of corresponding activation in the occluded quadrant.

4.3. Multivariate pattern analysis (MVPA)

The MVPA analyses were designed to identify potential shape or identity information represented during occlusion. Classifiers were trained to discriminate objects (circles vs. stars) during both flashing and dynamic occlusion. Because the flashing condition appeared in both experimental sessions (disappearance and dynamic occlusion), the reported results are the average classification performance across both sessions. There was no significant difference in shape classification performance for flashing objects across sessions (all ps > 0.47, two-sided Wilcoxon rank sum test). When using the flashing data to train for cross-classification with data from the motion condition, only the flashing data from the corresponding session were used (i.e., flashing data from the disappearance session were used to classify object shape when objects disappeared and flashing data from the occlusion session were used to classify object shape when objects were dynamically occluded).

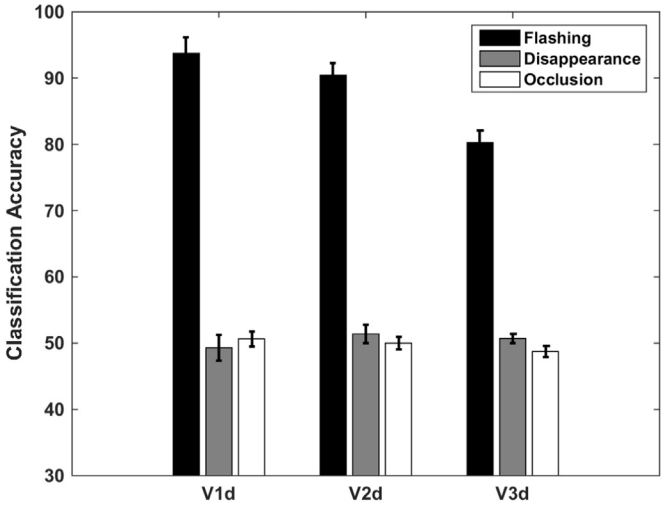

Fig. 4. Shape classification performance of circles vs. stars for three classifiers. The black bars show performance for a classifier trained on flashing and tested on flashing stimuli, with performance averaged across the two testing sessions. The gray bars indicate cross-classification performance of a classifier trained on the flashing stimuli, but tested on the motion stimuli that disappeared. The white bars are the same as the gray, but for gradually occluding motion stimuli. Error bars are standard errors.

Classifier performance for dorsal regions of left hemisphere V1-V3 corresponding to occlusion quadrant are shown in Fig. 4. Circle and star patterns of activation could readily be discriminated in V1-V3 when the objects were physically present during flashing (all $p_{perm} < 0.05$; black bars). However, classification performance was not significantly different from chance (all $p_{perm} > 0.16$) in any ROI for either disappearing (gray bars) or occluded objects (white bars). Although there was enough discriminatory power in V1-V3 to decode object identity when the objects were physically present (a classifier trained and tested on (withheld) flashing shapes), there was not enough information to do so when they were dynamically occluded (cross-classification: trained on flashing, tested on occluded), even though there was corresponding activation for gradually occluded objects (Fig. 3).

As a sanity check, a classifier was also trained and tested on motion data, i.e. when the shapes were fully visible in the motion quadrants (upper-right and lower-left). If shapes could not be discriminated while visible, it would have been unlikely that they could be when invisible in the occlusion quadrant. Object shapes were discriminable above chance (all $p_{perm} < 0.005$) in all ROIs for both the upper-right and lower-left quadrants in both sessions (disappearance and occlusion). The lack of discriminability when cross-classifying was therefore not likely to be due lack of discriminatory power for moving shapes.

The cross-classification used data from the flashing condition for training and data from the motion conditions for testing, essentially only using half of the available data. The correlation analysis measuring shape information may be a more powerful analysis because it uses all available data. The results of the correlation analysis for V1-V3 are shown in Fig. 5. A one-sample bootstrap hypothesis test found no evidence shape information in the occluded quadrant in any ROI. Δr was statistically significantly different from zero for stars in V2 ($p < 0.035$, 95% CI=[−0.237, −0.045]); however, this measure was negative, indicating that the pattern of activation of moving stars was more similar to flashing circles than to flashing stars. It is not clear why there was this negative correlation, but it does not reflect shape information, which would require a positive correlation. Taken together, the MVPA and correlation analyses suggest that although there is increased activity in early visual cortex during dynamic occlusion, there is no evidence that this activity reflects the representation of shape or identity information about the objects.

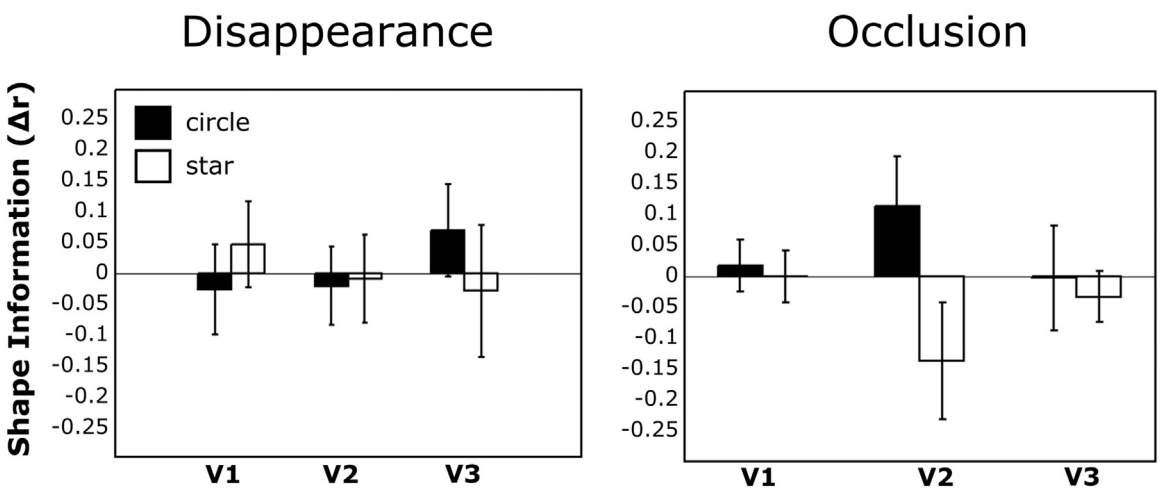

Fig. 5. Shape information, Δ*r*, for dorsal visual areas in the left hemisphere, corresponding to the lower-right, occlusion quadrant for circles (black) and stars (white) and for the disappearance (left) and occlusion (right) conditions. Error bars are standard errors.

4.4. Representation of object identity in higher visual areas

The same analyses were carried out for all ROIs beyond V1-V3. However, neurons in these higher-order areas have large receptive fields that can span entire hemifields (Amano et al., 2009; Grill-Spector and Malach 2004; Larsson and Heeger 2006; Malach et al. 1995; Swisher et al. 2007; Wandell et al., 2007) and may therefore respond to stimuli in other quadrants than the occlusion quadrant of interest during the motion condition because objects were visible in the upper-right and lower-left quadrants before disappearing or becoming gradually occluded in the lower-right quadrant. In order to mitigate these effects, voxels were selected by using a flashing > motion contrast. This limited the number of voxels that could have been driven by the presence of physically moving object in the other quadrants.

The results of the MVPA cross-classification (trained on flashing, tested on motion) are shown in Fig. 6. Object identity could be decoded during dynamic occlusion in several ROIs including: VO1 (p_{perm}=0.0167), VO2 (p_{perm}=0.0116), LO2 (p_{perm}=0.0217), TO1 (p_{perm}=0.0042), TO2 (p_{perm}=0.0012), LOC (p_{perm}=0.0004) and hMT+ (p_{perm}=0.0027) for disappearing objects (FDR=0.1) and in VO1 (p_{perm}=0.0170), VO2 (p_{perm}=0.0020), PHC1 (p_{perm}=0.0016), LO2 (p_{perm}=0.0007), TO1 (p_{perm}=0.0002), TO2 (p_{perm}=0.0277), IPS4 (p_{perm}=0.0424), FFA (p_{perm}=0.0079), PPA (p_{perm}=0.0001), LOC (p_{perm}=0.0003), and hMT+ (p_{perm}=0.0157) when the objects were occluded (FDR=0.018). As a control, the same analysis was applied to ROIs from the right hemisphere which also included moving stimuli (lower-left quadrant) and had flashing stimuli in the control quadrant. If shape classification in the left hemisphere was driven by voxels with large receptive fields that were responding to visible, moving objects in the upper-right quadrant, then similar classification performance may be expected for voxels in the upper-left control quadrant with large receptive fields that span into the lower-left quadrant in which moving objects were also visible. However, shapes could only be discriminated from activity in the right hemisphere in VO2, LO2, V3a and LOC for disappearing objects (FDR=0.2) and in PHC2, LO1, TO1, and IPS3 for gradually occluded objects (FDR=0.1) and in no other ROIs in which they were discriminable for the left hemisphere (Fig. S5). This suggests that classification performance in these higher-level ROIs were not primarily driven by activation of voxels that were responding to the moving shapes when they were visible and instead that these areas are encoding shape identity information during dynamic occlusion. The timecourse and correlation analyses were also performed for these ROIs and are described in the supplementary materials.

5. Discussion

We examined cortical activity throughout visual cortex during the perception of dynamic occlusion in order to determine whether neural representations of occluded objects maintained form information or were more token-like. Our primary result is that the univariate activation timecourses within unstimulated regions of V1-V3 revealed a corresponding signal for gradually occluded, but not for disappearing shapes. However, subsequent multivariate analyses found no evidence that this activity reflected shape identity information. Instead, we found evidence for shape identity information in several higher-order, topographically organized visual areas, as well as in functionally defined areas hMT+, LOC, PPA and FFA.

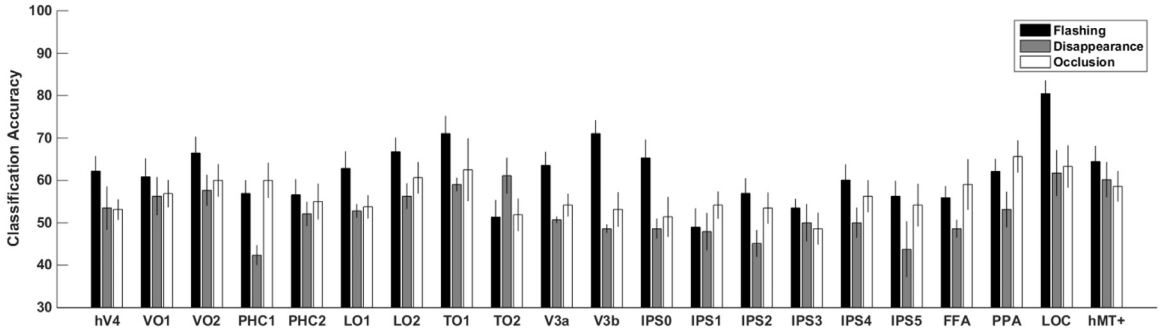

Fig. 6. Average classification accuracy for objects in ROIs in higher visual areas. The black bars show performance for a classifier trained on flashing and tested on flashing stimuli, with performance averaged across the two testing sessions. The gray bars indicate cross-classification performance of a classifier trained on the flashing stimuli, but tested on the motion stimuli that disappeared. The white bars are the same as the gray, but for gradually occluding motion stimuli. Error bars are standard errors.

It may come as a surprise that no univariate effect was observed for the instantaneously disappearing conditions. The block design of the experiment lead the stimuli to be on the screen for a long time, their motion-path was repeatedly shown, several subjects reported experiencing apparent motion across the target quadrant, and the use of a block design afforded every opportunity to fill in an interpolated motion path in a top-down way. This stands in contrast to several other studies of representations along the apparent motion path that have found increased activity in early visual cortex (Goebel et al., 1998; Larsen et al., 2006; Maus et al., 2010; Muckli et al., 2005; Seghier et al., 2000; Sterzer et al., 2006; Wibral et al., 2008). However, a similar lack of activation was also observed in a recent study of representations along the apparent motion path (Chong et al., 2015). The use of circle and star stimuli was intended to minimize the contribution of orientation-specific horizontal processing within and between early visual areas including V1 (Field et al., 1993; Fregnac et al., 2009; Gilbert et al., 1996; Seriès et al., 2002; Seriès et al., 2003). It may be the case that past findings of increased activity along the path of apparent motion arose from such local horizontal interactions and not from long-range feedback from higher order areas. Indeed, several of these past finding used oriented stimuli that are likely to activate these horizontal mechanisms (Chong et al., 2015; Muckli et al., 2005; Schwarzkopf et al., 2011; Sterzer et al., 2006). This is not to say that feedback does not play a role in either apparent motion or dynamic occlusion. Several studies have demonstrated that feedback from hMT+, for example, is critical for the perception of motion in apparent motion (Liu et al., 2004; Matsuyoshi et al., 2007; Sterzer et al., 2006; Vetter et al., 2015; Wibral et al., 2008). Similar feedback may be responsible for the activation we observed during dynamic occlusion in V1-V3. However, the phenomenological experience of apparent motion in our disappearance condition is subtle, and some participants reported not experiencing apparent motion at all. Thus the lack of a univariate signal for disappearing stimuli may simply be because, in general, any apparent motion signal that was present was either too weak or too inconsistent to detect.

A univariate signal was observed for dynamically occluded stimuli in early visual areas (V1-V3). However, subsequent multivariate analyses revealed that this signal did not carry information about the dynamically occluded object's shape identity. This null result again highlights a key difference with observations from experiments using apparent motion. A recent finding concluded that during apparent motion, orientation information is encoded along the motion path in V1 (Chong et al., 2015). In their study, apparent motion was induced between two orientated gratings. The orientation of the interpolated grating could either be parallel or orthogonal to the apparent motion path depending on a cue. The cue induced differentiable responses in V1 across several orientation channels. However, the tuning of the channels was broad, varying by ± 45° and the tuning curves for the apparent motion path region of interest did not match the interpolated orientations for their two conditions. The tuning curve for the vertical condition (90°) peaked at 112.5° and the horizontal condition (180°) peaked at 135°; a relative offset from each other of 22.5° despite a targeted difference of 90°. It is therefore unclear the extent to which the observed patterns of activity reflected filled-in orientation. Furthermore, this study, like several others that have examined activations along the path of apparent motion, employed oriented Gabor-like stimuli.

Why was there activity in early visual cortex during dynamic occlusion if that activity did not carry distinguishing orientation or shape information? Extensive feedback projections from higher to lower visual areas may pass a diverse variety of information (see Kravitz et al. (2013) for a review). For example, feedback signals are sent from motion area hMT+/V5 to V1 (Ahmed et al., 2008; Alink et al., 2010; Muckli et al., 2005; Sterzer et al., 2006; Vetter et al., 2015; Wibral et al., 2008), and attention (Fang et al., 2008; Lee et al., 2002; Müller and Kleinschmidt, 2003) and context (Lamme, 1995; Murray et al., 2006b; Zipser et al., 1996) can modulate activity in early visual areas. Recurrent connections and feedback from LOC to early visual cortex may be involved in the perception of form and illusory contours (Lamme and Roelfsema, 2000; Murray et al., 2004; Murray et al., 2006a; Scholte et al., 2008; Shpaneret al., 2013; Williams et al., 2008). The observed activity in early visual cortex may therefore reflect a representation of the object's motion path, the path of attention through that quadrant, or else information about a “salient region” – some thing that is moving through the occluded quadrant without specific shape identity information. Such representations may partially arise due to feedback from higher visual areas.

Taken together, our results suggest that object representations during dynamic occlusion may be more “Pylyshyn-esque” than “Kosslyn-esque”. Pylyshyn had previously argued for an object-file (FINST) or token-like representations of objects (Pylyshyn, 1989). When an object completely disappears, we are able to track and follow it, we represent its motion path and trajectory, updating its position, but we cease to accurately represent specific details about its shape. Instead, we maintain a more abstract representation of the object's identity, perhaps in higher-level visual areas, so that we may expect a similar-looking shape to later reemerge, but are not continuously storing precise information about its edges or orientation within early stages of visual processing. Similarly, in the case of long-range apparent motion, as long as spatiotemporal continuity is maintained, motion can readily be perceived between two successive presentations of objects that differ in shape, orientation, or color (Kolers and Pomerantz, 1971). Under this theory, the activation observed in early visual cortex may correspond to the motion path of the object or a “blob-like” representation of it during occlusion. Circles could not be discriminated from stars in those areas because the information about those shapes was not maintained at that representational level. This view stands in contrast to a Kosslyn-esque representational scheme which might be said to describe a rich representation for occluded and invisible objects. Early visual cortex has been found to be activated during visual imagery and it has been argued that visualization reactivates, via feedback, areas of cortex that would be active while actually viewing an object (Albers et al., 2013; Klein et al., 2000; Slotnick et al., 2005). Our findings support the notion of feedback from higher-level to lower-level cortical areas, but not at the proposed level of detailed representation. However, these representational regimes are not mutually exclusive. It is possible that some shape features are still maintained while an object is invisible and are represented in early visual cortex. The present design may have simply been too weak to detect such representations or else the nature of occlusions in this particular experiment (entire large and moving objects disappearing all at once in a large area) did not lend itself to the support of such representations.

In summary, we found cortical activity corresponding to a dynamically occluded object in early visual cortex. While this activity does not encode object identity, it may represent some property other than form, such as velocity, position (Akselrod et al., 2014), or global orientation (Hidaka et al., 2011). It is also possible that the activity reflects non-object related information such as information about the motion path itself (Schwarzkopf et al., 2011; Sterzer et al., 2006), or attention along the path (Culham et al., 1998). This suggests that during occlusion there may exist only a token- or FINST-like (Pylyshyn, 1989) representation of an object in early visual cortex. This representation would allow for tracking and correspondence across appearances, but would not retain specific form information. In contrast, shape identity information, if represented during occlusion is represented within higher-order visual areas. This lack of detailed information in early visual cortex may facilitate the perception of motion between perceptually distinct objects as in long-range apparent motion.

Acknowledgements

We would like to thank Ryan Mruczek and Kyle Killebrew for their assistance with this project. This work was supported by the National Eye Institute (R15EY022775 to G.P.C. and 1F32EY025520-01A1 to G.E.) and the National Institute of General Medical Sciences (1P20GM103650 to G.P.C.).

Appendix A. Supplementary material

Supplementary data associated with this article can be found in the online version at http://dx.doi.org/10.1016/j.neuroimage.2016.09.024.

References

Ahmed, B., Hanazawa, A., Undeman, C., Eriksson, D., Valentiniene, S., Roland, P.E., 2008. Cortical dynamics subserving visual apparent motion. Cereb. Cortex 18, 2796–2810.
Akselrod, M., Herzog, M.H., Öğmen, H., 2014. Tracing path-guided apparent motion in human primary visual cortex V1. Sci. Rep. 4, 1–5.
Albers, A.M., Kok, P., Toni, I., Dijkerman, H.C., de Lange, F.P., 2013. Shared representations for working memory and mental imagery in early visual cortex. Curr. Biol. 23, 1427–1431.
Alink, A., Schwiedrzik, C.M., Kohler, A., Singer, W., Muckli, L., 2010. Stimulus predictability reduces responses in primary visual cortex. J. Neurosci. 30, 2960–2966.
Amano, K., Wandell, B.A., Dumoulin, S.O., 2009. Visual field maps, population receptive field sizes, and visual field coverage in the human MT+ complex. J. Neurophysiol. 102, 2704–2718.
Arcaro, M.J., McMains, S.A., Singer, B.D., Kastner, S., 2009. Retinotopic organization of human ventral visual cortex. J. Neurosci. 29, 10638–10652.
Assad, J.A., Maunsell, J.H.R., 1995. Neuronal correlates of inferred motion in primate posterior parietal cortex. Nature 373, 518–521.
Attneave, F., 1974. Apparent movement and the what-where connection. Psychologia 17, 108–120.
Bahrami, B., 2003. Object property encoding and change blindness in multiple object tracking. Vis. Cogn. 10, 949–963.
Baker, C., Keysers, C., Jellema, T., Wicker, B., Perrett, D., 2001. Neuronal representation of disappearing and hidden objects in temporal cortex of the macaque. Exp. Brain Res 140, 375–381.
Ban, H., Yamamoto, H., Hanakawa, T., Urayama, S.-i, Aso, T., Fukuyama, H., Ejima, Y., 2013. Topographic representation of an occluded object and the effects of spatiotemporal context in human early visual areas. J. Neurosci. 33, 16992–17007.
Bandettini, P.A., Jesmanowicz, A., Wong, E.C., Hyde, J.S., 1993. Processing strategies for time-course data sets in functional MRI of the human brain. Magn. Reson. Med. 30, 161–173.
Benjamini, Y., Hochberg, Y., 1995. Controlling the false discovery rate: a practical and powerful approach to multiple testing. J. R. Stat. Soc.: Ser. B 57, 289–300.
Benjamini, Y., Yekutieli, D., 2001. The control of the false discovery rate in multiple testing under dependency. Ann. Stat. 29, 1165–1188.
Brainard, D.H., 1997. The psychophysics toolbox. Spat. Vis. 10, 433–436.
Brewer, A.A., Liu, J., Wade, A.R., Wandell, B.A., 2005. Visual field maps and stimulus selectivity in human ventral occipital cortex. Nat. Neurosci. 8, 1102–1109.
Burke, L., 1952. On the tunnel effect. Q. J. Exp. Psychol. 4, 121–138.
Caplovitz, G.P., Shapiro, A., Stroud, 2011. The maintenance and disambiguation of object representations depend upon feature contrast within and between objects. J. Vis. 11, 1–14.
Chong, E., Familiar, A.M., Shim, W.M., 2015. Reconstructing representations of dynamic visual objects in early visual cortex. Proc. Natl. Acad. Sci. USA.. http://dx.doi.org/10.1073/pnas.1512144113.
Cortes, C., Vapnik, V., 1995. Support-vector networks. Mach. Learn. 20, 273–297.
Cox, R.W., 1996. AFNI: software for analysis and visualization of functional magnetic resonance neuroimages. Comput. Biol. Res. 29, 162–173.
Culham, J.C., Brandt, S.A., Cavanagh, P., Kanwisher, N.G., Dale, A.M., Tootell, R.B.H., 1998. Cortical fMRI activation produced by attentive tracking of moving targets. J. Neurophysiol. 80, 2657–2670.
Dale, A.M., Fischl, B., Sereno, M.I., 1999. Cortical surface-based analysis. I. Segmentation and surface reconstruction. NeuroImage 9, 179–194.
DeYoe, E.A., Carman, G.J., Bandettini, P., Wieser, J., Cox, R., Miller, D., Neitz, J., 1996. Mapping striate and extrastriate visual areas in human cerebral cortex. Proc. Natl. Acad. Sci. USA 93, 2382–2386.
Engel, S.A., Glover, G.H., Wandell, B.A., 1997. Retinotopic organization in human visual cortex and the spatial precision of functional MRI. Cereb. Cortex 7, 183–192.
Epstein, R., Harris, A., Stanley, D., Kanwisher, N., 1999. The parahippocampal place area: recognition, navigation, or encoding? Neuron 23, 115–125.
Erlikhman, G., Keane, B.P., Mettler, E., Horowitz, T.S., Kellman, P.J., 2013. Automatic feature-based grouping during multiple object tracking. J. Exp. Psychol.: Hum. Percept. Perform. 39, 1628–1637.
Erlikhman, G., Gurariy, G., Mruczek, R.B., Caplovitz, G., 2016. The neural representation of objects formed through the spatiotemporal integration of visual transients. NeuroImage, (In Press).
Etzel, J.A., 2015. MVPA Permutation Schemes: Permutation Testing for the Group Level. In: Proceedings of the 5th International Workshop on Pattern Recognition in NeuroImaging. IEEE, Stanford, CA, USA.
Etzel, J.A., Braver, T.S., 2013. MVPA Permutation Schemes: Permutation Testing in the Land of Cross-Validation. In: Proceedings of the 3rd International Workshop on Pattern Recognition in Neuroimaging. IEEE, Philadelphia, PA.
Exner, S., 1875. Ueber das Segen von Bewegungen und die Theorie desZusammengesetzen Auges. Sitzungsberichte Akad. Wiss. Wien. 72, 156–190.
Fang, F., Boyaci, H., Kersten, D., Murray, S.O., 2008. Attention-dependent representation of size illusion in human V1. Curr. Biol. 18, 1707–1712.
Feldman, J., Tremoulet, P.D., 2006. Individuation of visual objects over time. Cognition 99, 131–165.
Field, D.J., Hayes, A., Hess, R.F., 1993. Contour integration by the human visual system: Evidence for a local "association field". Vis. Res. 33, 173–193.
Fischl, B., Sereno, M.I., Dale, A.M., 1999. Cortical surface-based analysis. II. Inflation, flattening, and a surface-based coordinate system. NeuroImage 9, 195–207.
Flombaum, J.I., Scholl, B.J., 2006. A temporal same-object advantage in the tunnel effect: Facilitated change detection for persisting objects. J. Exp. Psychol.: Hum. Percept. Perform. 32, 840–853.
Flombaum, J.I., Scholl, B.J., Santos, L.R., 2008. Spatiotemporal priority as a fundamental principle of object persistence. Orig. Object Knowl., 134–164.
Fregnac, Y., Baudot, P., Chavane, F., Lorenceau, J., Marre, O., Monier, C., Pananceau, M., Carelli, P.V., Sadoc, G., 2009. Multiscale functional imaging in V1 and cortical correlates of apparent motion. In Dynamics of visual motion processing. Springer, US, 73–93.
Friston, K.J., Frith, C.D., Turner, R., Frackowiak, R.S.J., 1995. Characterizing evoked hemodynamics with fMRI. NeuroImage 2, 157–165.
Gao, T., Scholl, B.J., 2010. Are objects required for object-files? Roles of segmentation and spatiotemporal continuity in computing object persistence. Vis. Cogn. 18, 82–109.
Gilbert, C.D., Das, A., Ito, M., Kapadia, M., Westheimer, G., 1996. Spatial integration and cortical dynamics. P. Nat. Acad. Sci. USA 93, 615–622.
Goebel, R., Khorram-Sefat, D., Muckli, L., Hacker, H., Singer, W., 1998. The constructive nature of vision: direct evidence from functional magnetic resonance imaging studies of apparent motion and motion imagery. Eur. J. Neurosci. 10, 1563–1573.
Grill-Spector, K., Kushnir, T., Hendler, T., Edelman, S., Itzchak, Y., Malach, R., 1998. A sequence of object-processing stages revealed by fMRI in the human occipital lobe. Hum. Brain Mapp. 6, 316–328.
Grill-Spector, K., Malach, R., 2004. The human visual cortex. Annu. Rev. Neurosci. 27, 649–677.
Halko, M.A., Mingolla, E., Somers, D.C., 2008. Multiple mechanisms of illusory contour perception. J. Vis. 8, 1–17.
Haxby, J.V., Ungerleider, L.G., Clark, V.P., Schouten, J.L., Hoffman, E.A., Martin, A., 1999. The effect of face inversion on activity in human neural systems for face and object perception. Neuron 22, 189–199.
Hein, E., Moore, C.M., 2012. Spatio-temporal priority revisited: The role of feature identity and similarity for object correspondence in apparent motion. J. Exp. Psychol.: Hum. Percept. Perform. 38, 975–988.
Hidaka, S., Nagai, M., Sekuler, A.B., Bennet, P.H., Gyoba, J., 2011. Inhibition of target detection in apparent motion trajectory. J. Vis. 11, 1–12.
Howard, C.J., Holcombe, A.O., 2008. Tracking the changing features of multiple objects: Progressively poorer perceptual precision and progressively greater perceptual lag. Vis. Res. 48, 1164–1180.
Hulme, O.J., Zeki, S., 2007. The sightless view: neural correlates of occluded objects. Cereb. Cortex 17, 1197–1205.
Kahneman, D., Treisman, A., Gibbs, B.J., 1992. The reviewing of object files: object-selective integration of information. Cogn. Psychol. 24, 175–219.
Kaneoke, T., Bundou, M., Koyama, S., Suzuki, H., Kakigi, R., 1997. Human cortical area responding to stimuli in apparent motion. NeuroReport 8, 677–682.
Kanwisher, N., Woods, R.P., Iacoboni, M., Mazziotta, J.C., 1997. A locus in human extrastriate cortex for visual shape analysis. J. Cogn. Neurosci. 9, 133–142.
Kastner, S., DeSimone, K., Konen, C.S., Szczepanski, S.M., Weiner, K.S., Schneider, K.A., 2007. Topographic maps in human frontal cortex revealed in memory-guided saccade and spatial working-memory tasks. J. Neurophysiol. 97, 3494–3507.
Keane, B.P., Mettler, E., Tsoi, V., Kellman, P.J., 2011. Attentional signatures of perception: multiple object tracking reveals the automaticity of contour interpolation. J Exp. Psychol.: Hum. Percept. Perform. 37, 685–698.
Killebrew, K., Mruczek, R., Berryhill, M.E., 2015. Intraparietal regions play a material general role in working memory: evidence supporting an internal attentional role. Neuropsychologia 73, 12–24.
Klein, I., Paradis, A.L., Poline, J.B., Kosslyn, S.M., Le Bihan, D., 2000. Transient activity in the human calcarine cortex during visual-mental imagery: An event-related fMRI study. J. Cogn. Neurosci. 12, 15–23.
Kolers, P.A., 1964. The illusion of movement. Sci. Am. 211, 98–106.
Kolers, P.A., Pomerantz, J.R., 1971. Figural change in apparent motion. J. Exp. Psychol. 87, 99–108.
Konen, C.S., Kastner, S., 2008. Representation of eye movements and stimulus motion in topographically organized areas of human posterior parietal cortex. J. Neurosci. 28, 8361–8375.
Korte, A., 1915. Kinematoscopishe Untersuchungen. Seitzscrhift für Psychol. 72, 193–206.
Kravitz, D.J., Saleem, K.S., Baker, C.I., Ungerleider, L.G., Mishkin, M., 2013. The ventral visual pathway: an expanded neural framework for the processing of object quality. Trends Cogn. Sci. 17, 26–49.
Krzywinski, M., Altman, N., 2014. Comparing samples – Part II. Nat. Methods 11,

355–356.
Lamme, V.A.F., 1995. The neurophysiology of figure-ground segregation in primary visual cortex. J. Neurosci. 15, 1605–1615.
Lamme, V.A.F., Roelfsema, P.R., 2000. The distinct modes of vision offered by feedforward and recurrent processing. Trends Neurosci. 23, 571–579.
Larsen, A., Madsen, K.H., Lund, T.E., Bundesen, C., 2006. Images of illusory motion in primary visual cortex. J. Cogn. Neurosci. 18, 1174–1180.
Larsson, J., Heeger, D.J., 2006. Two retinotopic visual areas in human lateral occipital cortex. J. Neurosci. 26, 13128–13142.
Lee, T.S., Yang, C.F., Romero, R.D., Mumford, D., 2002. Neural activity in early visual cortex reflects behavioral experience and higher-order perceptual saliency. Nature 5, 589–597.
Liu, T., Slotnick, S.D., Yantis, S., 2004. Human MT+ mediates perceptual filling-in during apparent motion. NeuroImage 21, 1772–1780.
Makin, A.D., Poliakoff, E., El-Deredy, W., 2009. Tracking visible and occluded targets: Changes in event related potentials during motion extrapolation. Neuropsychologia 47, 1128–1137.
Malach, R., Reppas, J.B., Benson, R.R., Kwong, K.K., Jiang, H., Kennedy, W.A., Ledden, P.J., Brady, T.J., Rosen, B.R., Tootell, R.B.H., 1995. Object-related activity revealed by functional magnetic resonance imaging in human occipital cortex. Proc. Natl. Acad. Sci. USA 92, 8135–8139.
Marr, D., 1982. Vision. W H Freeman, San Francisco, CA.
Matsuyoshi, D., Hirose, N., Mima, T., Fukuyama, H., Osaka, N., 2007. Repetitive transcranial magnetic stimulation of human MT+ reduces apparent motion perception. Neurosci. Lett. 429, 131–135.
Maus, G.W., Weigelt, S., Nijhawan, R., Muckli, L., 2010. Does area V3A predict positions of moving objects? Front. Psychol. 1, 186. http://dx.doi.org/10.3389/fpsyg.2010.00186.
Michotte, A., Thinès, G., Crabbé, G., 1964. Les complements amodaux des structures perceptives. Institut de psychologie de l'Université de Louvain.
Muckli, L., Kohler, A., Kriegeskorte, N., Singer, W., 2005. Primary visual cortex activity along the apparent-motion trace reflects illusory perception. PLOS Biol. 3, e265.
Müller, N.G., Kleinschmidt, A., 2003. Dynamic interaction of object- and space-based attention in retinotopic visual areas. J. Neurosci. 23, 9812–9816.
Murray, M.M., Foxe, D.M., Javitt, D.C., Foxe, J.J., 2004. Setting boundaries: brain dynamics of modal and amodal illusory shape completion in humans. J. Neurosci. 24, 6898–6903.
Murray, M.M., Imber, M.L., Javitt, D.C., Foxe, J.J., 2006a. Boundary completion is automatic and dissociable from shape discrimination. J. Neurosci. 26, 12043–12054.
Murray, S.O., Boyaci, H., Kersten, D., 2006b. The representation of perceived angular size in human primary visual cortex. Nat. Neurosci. 9, 429–434.
Navon, D., 1976. Irrelevance of figural identity for resolving ambiguities in apparent motion. J Exp. Psychol. 2, 130–138.
Oksama, L., Hyönä, J., 2008. Dynamic binding of identity and location information: a serial model of multiple identity tracking. Cogn. Psychol. 56, 237–283.
Olson, I.R., Gatenby, K.C., Leung, H.-C., Skudlarski, P., Gore, J.C., 2003. Neuronal representation of occluded objects in the human brain. Neuropsychologia 45, 95–104.
Palmer, E.M., Kellman, P.J., Shipley, T.F., 2006. A theory of dynamic occluded and illusory object perception. J. Exp. Psychol. 135, 515–541.
Papenmeier, F., Meyerhoff, H.S., Jahn, G., Huff, M., 2013. Tracking by location and features: Object correspondence across spatiotemporal discontinuities during multiple object tracking. J. Exp. Psychol.: Hum. Percept. Perform. 40, 159–171.
Peelen, M.V., Fei-Fei, L., Kastner, S., 2009. Neural mechanisms of rapid natural scene categorization in human visual cortex. Nature 460, 94–97.
Pelli, D.G., 1997. The videotoolbox software for visual psychophysics: transforming numbers into movies. Spat. Vision. 10, 437–442.
Prazdny, K., 1986. What variables control (long-range) apparent motion? Perception 15, 37–40.
Press, W.A., Brewer, A.A., Dougherty, R.F., Wade, A.R., Wandell, B.A., 2001. Visual areas and spatial summation in human visual cortex. Vis. Res. 41, 1321–1332.
Pylyshyn, Z.W., 1989. The role of location indexes in spatial perception: a sketch of the FINST spatial-index model. Cognition 32, 65–97.
Pylyshyn, Z.W., 2001. Visual indexes, preconceptual objects, and situated vision. Cognition 80, 127–158.
Pylyshyn, Z.W., 2004. Some puzzling findings in multiple object tracking: I. Tracking without keeping track of object identities. Vis. Cogn. 11, 801–822.
Saad, Z., Reynolds, R., Cox, R.J., Argall, B., Japee, S., 2004. SUMA: an interface for surface-based intra- and inter-subject analysis. I S Biomed. Imaging, 2004, pp. 1510–1513.
Saiki, J., 2003. Feature binding in object-file representations of multiple moving items. J. Vis. 3, 6–21.
Scholl, B.J., Pylyshyn, Z.W., 1999. Tracking multiple items through occlusion: clues to visual objecthood. Cogn. Psychol. 38, 259–290.
Scholte, H.S., Jolij, J., Fahrenfort, J.J., Lamme, V.A.F., 2008. Feedforward and recurrent processing in scene segmentation: electroencephalography and functional magnetic resonance imaging. J. Cogn. Neurosci. 20, 2097–2109.
Schwarzkopf, D.S., Sterzer, P., Rees, G., 2011. Decoding of coherent but not incoherent motion signals in early dorsal visual cortex. NeuroImage 56, 688–698.
Seghier, M., Dojat, M., Delon-Martin, C., Rubin, C., Warnking, J., Segebarth, C., Bullier, J., 2000. Moving illusory contours activate primary visual cortex: an fMRI study. Cereb. Cortex 10, 663–670.
Sereno, M.I., Dale, A.M., Reppas, J.B., Kwong, K.K., Belliveau, J.W., Brady, T.J., Rosen, B.R., Tootell, R.B.H., 1995. Borders of multiple visual areas in humans reveled by functional resonance imaging. Science 268, 889–893.
Seriès, P., Georges, S., Lorenceau, J., Frégnac, Y., 2002. Orientation dependent modulation of apparent speed: a model based on the dynamics of feed-forward and horizontal connectivity in V1 cortex. Vis. Res. 42, 2781–2797.
Seriès, P., Lorenceau, J., Frégnac, Y., 2003. The "silent" surround of V1 receptive fields: theory and experiments. J. Physiol. 97, 453–474.
Shipley, T.F., Kellman, P.J., 2003. Boundary completion in illusory contours: interpolation of extrapolation? Perception 32, 985–999.
Shpaner, M., Molholm, S., Forde, E., Foxe, J.J., 2013. Disambiguating the roles of area V1 and lateral occipital complex (LOC) in contour integration. NeuroImage 69, 146–156.
Shuwairi, S.M., Curtis, C.E., Johnson, S.P., 2007. Neural substrates of dynamic object occlusion. J. Cogn. Neurosci. 19, 1275–1285.
Singh, M., Fulvio, J.M., 2007. Bayesian contour extrapolation: geometric determinants of good continuation. Vis. Res. 47, 783–798.
Silver, M.A., Kastner, S., 2009. Topographic maps in human frontal and parietal cortex. Trends Cogn. Sci. 13, 488–495.
Slotnick, S.D., Thompson, W.L., Kosslyn, S.M., 2005. Visual mental imagery induces retinotopically organized activation of early visual areas. Cereb. Cortex 15, 1570–1583.
Stanley, D.A., Rubin, N., 2003. fMRI activation in response to illusory contours and salient regions in the human lateral occipital complex. Neuron 31, 323–331.
Stanley, D.A., Rubin, N., 2005. Rapid detection of salient regions: evidence from apparent motion. J. Vis. 5, 690–701.
Sterzer, P., Haynes, J.-D., Rees, G., 2006. Primary visual cortex activation on the path of apparent motion is mediated by feedback from hMT+/V5. NeuroImage 32, 1308–1316.
Storey, J.D., 2002. A direct approach to false discovery rates. J. R. Stat. Soc. B 64, 479–498.
Storey, J.D., Tibshirani, R., 2003. Statistical significance for genomewide studies. Proc. Natl. Acad. Sci. USA 100, 9440–9445.
Swisher, J.D., Halko, M.A., Merabet, L.B., McMains, S.A., Somers, D.C., 2007. Visual topography of human intraparietal sulcus. J. Neurosci. 27, 5326–5337.
Ullman, S., 1980. The effect of similarity between line segments on the correspondence strength in apparent motion. Perception 9, 617–626.
Vetter, P., Grosbras, M.-H., Muckli, L., 2015. TMS over V5 disrupts motion prediction. Cereb. Cortex 25, 1052–1059.
Wade, A.R., Brewer, A.A., Rieger, J.W., Wandell, B.A., 2002. Functional measurements of human ventral occipital cortex: retinotopy and colour. Philos. Trans. R. Soc. B 357, 963–973.
Wandell, B.A., Dumoulin, S.O., Brewer, A.A., 2007. Visual field maps in human cortex. Neuron 56, 366–383.
Wandell, B.A., Winawer, J., 2011. Imaging retinotopic maps in the human brain. Vis. Res. 51, 718–737.
Wang, L., Mruczek, R.E.B., Arcaro, M.J., Kastner, S., 2015. Probabilistic maps of visual topography in human cortex. Cereb. Cortex, bhu277.
Wertheimer, M., 1912. Experimentelle Studien uber das Sehen von Bewegungen. Zeritschrift für Psychol. 61, 161–265.
Wibral, M., Bledowski, C., Kohler, A., Singer, W., Muckli, L., 2008. The timing of feedback to early visual cortex in the perception of long-range apparent motion. Cereb. Cortex 19, 1567–1582.
Williams, M.A., Baker, C.I., Op de Beeck, H.P., Shim, W.M., Dang, S., Triantafyllou, C., Kanwisher, N., 2008. Feedback of visual object information to foveal retinotopic cortex. Nat. Neurosci. 11, 1439–1445.
Yantis, S., Nakama, T., 1998. Visual interactions in the path of apparent motion. Nat. Neurosci. 1, 508–512.
Zipser, K., Lamme, V.A.F., Schiller, P.H., 1996. Contextual modulation in primary visual cortex. J. Neurosci. 16, 7376–7389.